JOURNAL OF APPLIED ELECTROCHEMISTRY 11 (1981) 715–721

The impedance of the alkaline zinc-manganese dioxide cell. II. An interpretation of the data

S. A. G. R. KARUNATHILAKA, N. A. HAMPSON

Department of Chemistry, University of Technology, Loughborough, Leicestershire, LE11 3TU, UK

R. LEEK

Department of Electronic and Electrical Engineering, University of Technology, Loughborough, Leicestershire, LE11 3TU, UK

T. J. SINCLAIR

Procurement Executive, Ministry of Defence, Royal Armament Research and Development Establishment, Fort Halstead, Sevenoaks, Kent, UK

Received 13 January 1981

The impedance of small alkaline zinc–manganese dioxide cells has been interpreted in terms of a controlling charge-transfer and diffusion process at the zinc electrode throughout the early stages of discharge. After about 20% of the available charge has been removed, it becomes necessary to include the manganese dioxide electrode circuit components. This network has the circuit elements for charge transfer and a proceeding chemical reaction. The Warburg component for the manganese dioxide electrode need not be considered since the effective area considerably exceeds that of the zinc. The relative areas are confirmed by the magnitudes of the circuit element components. The decomposition of the impedance data has been successfully accomplished as far as 80% discharge; after this point cells show considerable differences from cell to cell, especially in the low-frequency range, which makes a confident interpretation difficult. It is considered that this is due to the loss of the physical definition of the system.

Nomenclature

C_m, C_z	double-layer capacitances of MnO_2 and Zn electrodes, respectively
C_X, R_X	parallel branch accounting for current density varying with fractional electrode coverage
R_Ω	resistance of electrolyte
V	open-circuit voltage of cell
Z, Z', Z''	impedance of cell, resistive component of Z and reactive component of Z, respectively
θ_m, θ_z	transfer resistance of MnO_2 and Zn electrodes, respectively
$\sigma, \sigma_R, \sigma_C$	in Warburg equation: $Z_W = \sigma\omega^{-1/2}(1 - i)$ or $Z_W = \sigma_R\omega^{-1/2} - i\sigma_C\omega^{-1/2}$.

1. Introduction

In Part 1 [1] we presented data showing how the impedance of alkaline zinc–manganese dioxide cells (Mallory, type MN1500) changed upon discharging from a very simple spectrum, characteristic of a process rate-controlled by a single charge-transfer step followed by diffusion in solution, when the cells were undischarged, to spectra of considerable complexity when the major part of the rated capacity of the cell had been withdrawn. We deferred the complete interpretation of data because our initial objective was to discover if the impedance of the cell could be used as an indication of the state-of-charge, as in the case of the Leclanché cell [2]. We now return to the interpretation of the data.

0021–891X/81/060715–07$02.70/0

2. The electrode processes

The processes which occur at the zinc and manganese dioxide electrodes have been investigated thoroughly over the past 20 years. The most recent account of these researches is given in the review edited by Barak and written by Tye [3]. It is clear from this review that it is now agreed that the reaction at the alkaline Zn electrode is relatively slow and might be expected initially to be the rate-controlling reaction in the cell. As the discharge continues (it is clear that) the manganese dioxide first goes through an Mn(III) stage and ultimately the reduction proceeds to the Mn(II) stage [3]. The zinc electrode becomes oxidized to zinc oxide and the mechanism does not change until solution conditions are such that ZnO is deposited at the electrode. It is unlikely that the zinc discharge mechanism changes merely by substituting one positive electrode for another so we are forced to conclude that the complex shape change in Sluyters plots reported in our earlier contribution must be due to the manganese dioxide (positive) electrode.

Recent work on the Zn–HgO system, however, suggests that this latter process does not have a significant effect on the impedance of the cell. In the Zn–HgO cell, it was found that the experimental data could be explained by simple charge-transfer and mass transport in solution at a controlling zinc electrode. This was accompanied by a progressive quasi-reversible transformation of HgO into Hg.

3. The model

In tackling this system it was considered that both electrodes must be taken into account and that the model for the zinc electrode was the simple Randles one [4], as shown in Fig. 1a. The electrochemistry of the manganese dioxide electrode is summarized by the equations

$$MnO_2 + H_2O + e \rightarrow MnOOH + OH^- \quad (1)$$

$$MnOOH + H_2O + e \rightarrow Mn(OH)_2 + OH^-. \quad (2)$$

Reaction 2 occurs to a large extent in the latter parts of the discharge and is more complex than shown in Equation 2, the mechanism being

$$MnOOH + H_2O \rightarrow Mn^{3+} + 3OH^- \quad (3)$$

$$Mn^{3+} + e \rightarrow Mn^{2+} \quad (4)$$

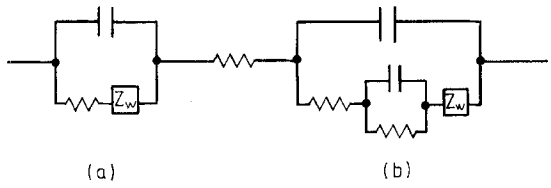

Fig. 1. (a) Simple Randles circuit; (b) Gerischer's coupled reaction circuit.

$$Mn^{2+} + 2OH^- \rightarrow Mn(OH)_2. \quad (5)$$

Equations 3–5 imply following and preceding reactions to the charge transfer. These have been shown by Gerischer [5, 6] to result in circuit elements of the type shown in Fig. 1b. The additional elements representing the chemical processes are in series with the Warburg impedance and the electron transfer and consequently appear in that connection as shown. Had the additional process, which increasingly appears as discharge continues, been in parallel with the electrode reaction as a reaction in the adsorbed state, then the circuit elements would have paralleled the original electrode reaction and the double layer, as shown convincingly by the classical work of Laitinen and Randles [7]. The complete electrical analogue of the cell is that shown in Figs. 1a and b.

4. The mathematical procedure

The procedure adopted was to write the complex equations for the resistive and capacitive components of the electrode (cell) impedance and to obtain a general solution for each of the c circuit elements. The equation for the impedance components (e.g. R) is expanded about approximate values (x') of the circuit elements (x) such that

$$x = x' + \Delta x \quad (6)$$

using Taylor's theorem, neglecting the second and higher order terms to obtain a linear equation

$$R = R' + \sum_c (dR/dx)'\Delta x. \quad (7)$$

The values of R' and the differentials can be calculated by the substitution of the approximate values of x in the expressions for R and the respective differential coefficients at each of the n experimental data points.

This gives n linear equations whose number is

reduced by the method of least squares to the c normal equations needed to isolate values of Δx for each circuit component. The approximate value of x is then corrected by adding Δx and the process is repeated until Δx is very small, i.e. effectively no variation in x. From this procedure we obtain the unknown circuit elements to a precision sufficient for comparison with the experimental data over the whole range.

The mathematical analysis of the impedance was carried out by writing the vector equation for each system. The calculation and isolation of the real (Z') and imaginary ($-Z''$) parts of the impedance were performed using the complex-number handling capability of the computer (PRIME 400). Using the technique given above, the most satisfactory correspondence between proposed and actual impedance data was tested.

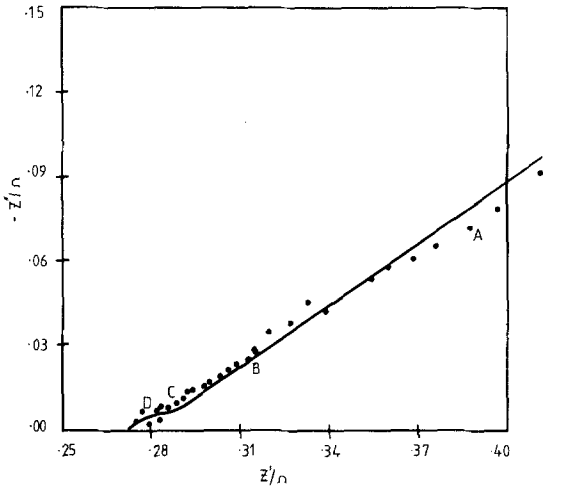
 ·15
·12
·09
·06
·03
·00
-Z''/Ω
·25
·28
·31
·34
·37
·40
Z'/Ω
A
B
C
D

Fig. 3. Complex-plane plot for new alkaline Zn–MnO_2 cell (MN1500) at 23°C. •, Experimental points; full line, computed behaviour (Fig. 1a). In Figs 3–11, A = 0.03 Hz, B = 0.31 Hz, C = 3.1 Hz, D = 31.2 Hz, E = 312 Hz and F = 3120 Hz.

5. Results

The general form of the impedance behaviour at different states of charge has already been described [1]. It was found that the data could generally be fitted into a scheme based on an analogue of the type shown in Fig. 2. Here the first circuit network is present at all states of charge; however, as charge is progressively drained from the cell, the second circuit network makes its appearance. This cell analogue applies until almost all the rated charge (~80%) has been drained from the cell. We would have expected a Warburg component in the reaction line of the network (Fig. 2b). This was never found to be present even at very high states of discharge. The decomposition of the experimental data into the elements of the circuit shown in Fig. 2 is shown in Figs. 3–11 for various states of discharge up to 80%.

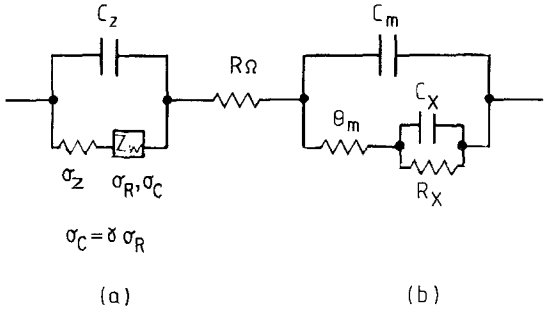
 C_z
C_m
RΩ
C_X
θ_m
Z_w
σ_z
σ_R, σ_C
R_X
$\sigma_C = \delta\,\sigma_R$
(a)
(b)

Fig. 2. (a) and (b) The cell analogue.

A difficulty of representation in these figures (Sluyters plots) is that the calculated and experimental curves may not be coincidental with respect to the frequency parameter. That this was so was checked by Randles plots and Figs. 12 and 13 show satisfactory conformation for a simple case at 20% discharged and at a very much greater state of discharge.

Table 1 contains the eight kinetic and physical constants which represent the cell behaviour in our experimental frequency range from 10 kHz. It

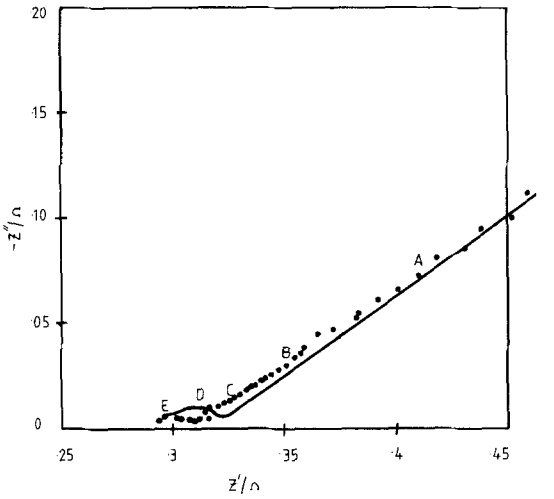
 20
15
10
05
0
-Z''/Ω
25
3
35
4
45
Z'/Ω
A
B
C
D
E

Fig. 4. As Fig. 3; 5% discharged.

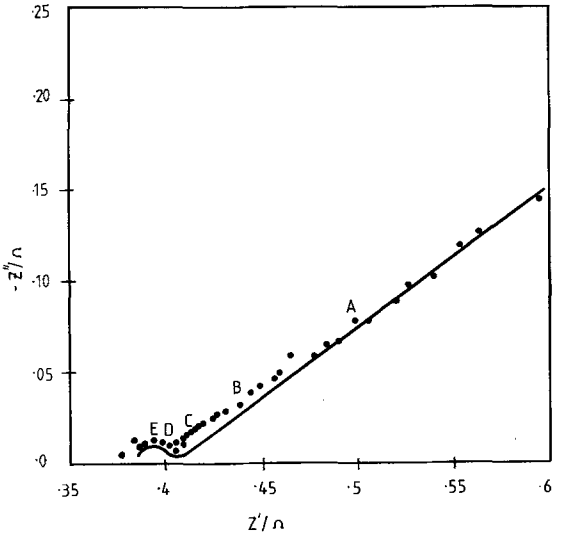

Fig. 5. As Fig. 3; 10% discharged.

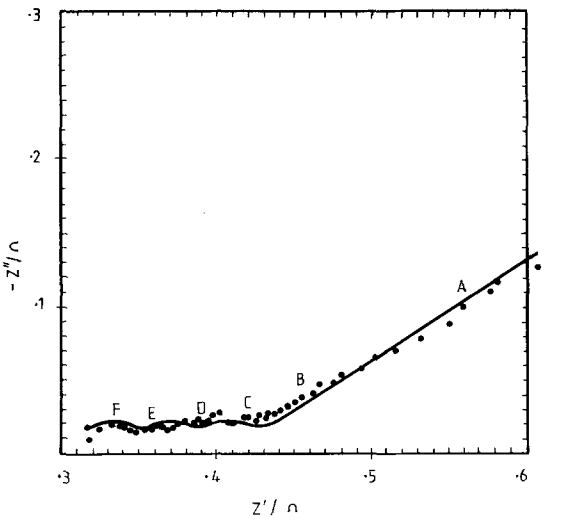

Fig. 7. As Fig. 3; 30% discharged.

should be noted in connection with the extraction of these data that the capacitance equation was very inefficient to use and in general we used the resistance equation. The reason for this was the relative magnitudes of the double-layer and Warburg contributions to the cell impedance. In the present case the Warburg contributions were very small in comparison with the double-layer values. This made it impossible to obtain good, uncertainty-free solutions on matrix inversion. For other cases (e.g. the alkaline Zn–HgO cell [8]) with a relatively much greater Warburg contribution this was not a disadvantage and both equations could be used with similar precision.

6. Discussion

The frequency spectra show good agreement between the theoretical predictions and the experimental data obtained with the model shown in Fig. 2. At all states of discharge the impedance behaviour ultimately becomes dominated by the Warburg impedance. This is an important point

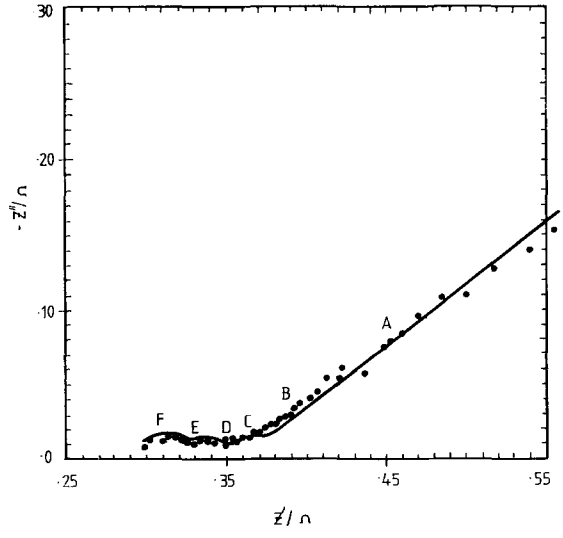

Fig. 6. As Fig. 3 but computed according to analogue of Figs. 1a and b; 20% discharged.

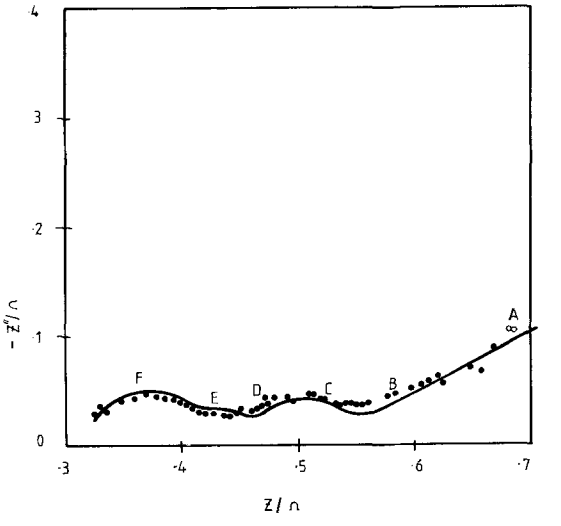

Fig. 8. As Fig. 3; 50% discharged.

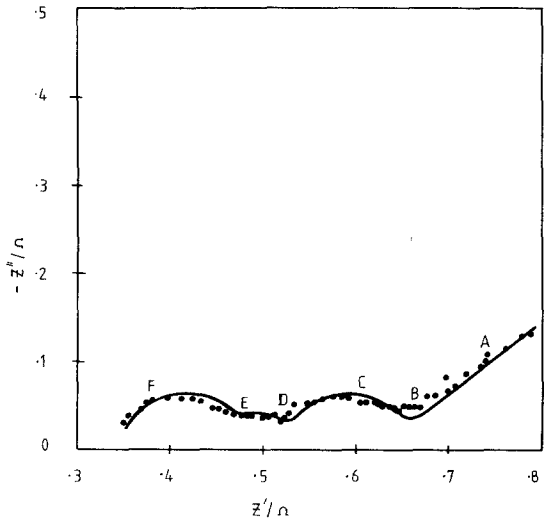

Fig. 9. As Fig. 3; 60% discharged.

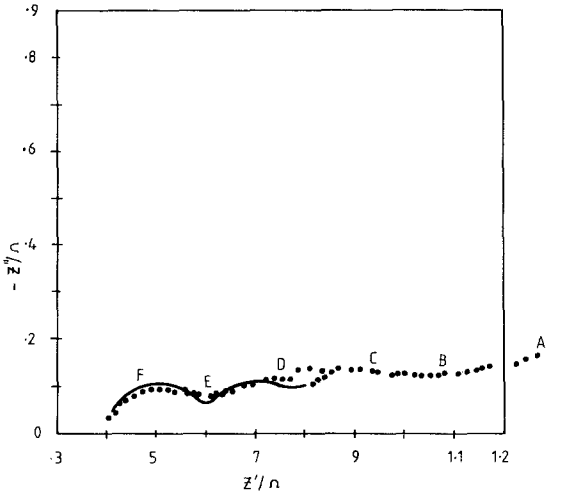

Fig. 11. As Fig. 3; 80% discharged.

operationally for, in the majority of applications, only Warburg components will need to be considered. Experimentally, however, the fine structure of the reaction and adsorption impedances are obscured so that the complete description of these cells is very difficult to obtain. It has become customary in examining the kinetic processes at single electrodes to remove the Warburg contribution by spinning the electrode at a high rotation speed. This is clearly impossible in the present case although it must be argued that our measurements are more relevant to the operational situation.

The interpretation of the cell behaviour follows from the electrode analogues necessary to describe the cell behaviour. When fully charged (new), the cell behaves as a simple charge-transfer and diffusion process. Indeed, in the frequency range experimentally available, a Warburg shape was only observed with a newly produced cell [1]. With stored cells, this was not the case and we interpret this as a deterioration in reactivity due to film formation within the cell. It is of interest to note that the second network in Fig. 2b does not contain a detectable Warburg component. We can interpret this if the area factor for the MnO_2 electrode is considerably greater than that of the zinc electrode so that the diffusion process is distributed over a much greater area. This is a

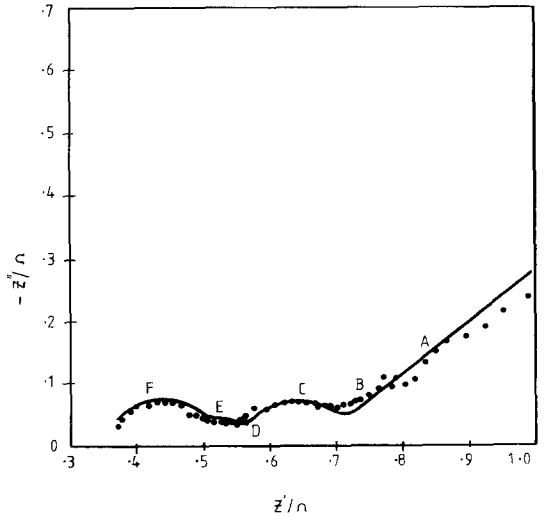

Fig. 10. As Fig. 3; 70% discharged.

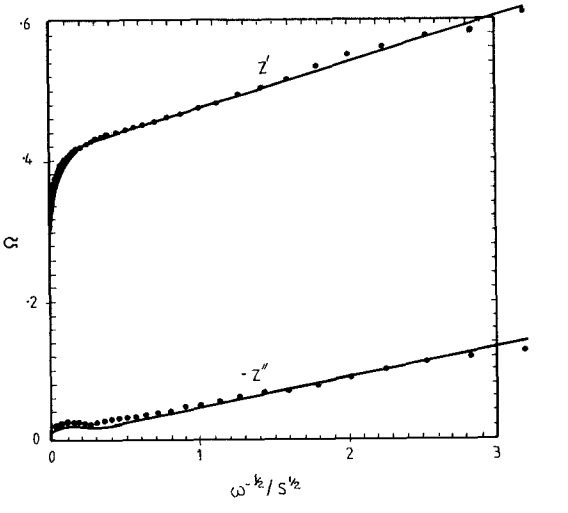

Fig. 12. Randles plot corresponding to Fig. 6.

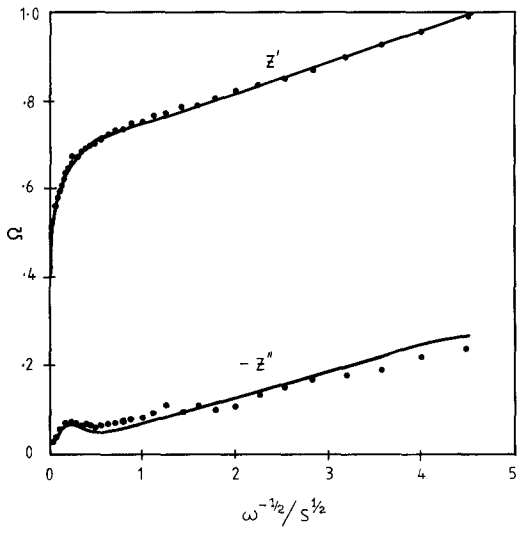

Fig. 13. Randles plot corresponding to Fig. 9.

likely explanation in view of the known physical properties of MnO_2, the admixture of the positive electrode MnO_2 with carbon and the use of mercury as an amalgamating agent in the case of the zinc.

When more than 80% of the available charge had been extracted from the cell, the impedance response from cell to cell became very inconsistent. This may be due to many reasons connected with uneven discharging and consequently it was not really possible to propose a satisfactory cell analogue. However, it is noteworthy that the inclusion of a Warburg factor in the MnO_2 network did not improve matters. Even at 80% discharge, Circuit 2 predicted a reactance component at a frequency lower than was actually observed. It was not possible to adjust this using any component representing any appropriate electrochemical process. We must conclude therefore that at low states of charge other undefined processes make their appearance (especially notable at low frequency) which complicate the impedance spectra in a fairly random manner. These are almost certainly connected with phase formation at the electrodes engendering part blocking and partially restricted or modified mass transport.

Table 1 shows the changes with discharging expected from our mechanism. The monotonic increase in the 'electrolyte resistance R_Ω' reflects the production of insulating ZnO and the removal of conducting MnO_2. θ_z and θ_m, the charge-transfer resistances for the electrodes, increase as the active ingredients are removed or coated with electrode products. Both double-layer capacitances reduce with discharging and it is satisfying to observe that $C_z < C_m$ in agreement with a larger surface area for the MnO_2 electrode than for the Zn under these conditions. It is not surprising that any Warburg component associated with the MnO_2 electrode remains undetected. R_X and C_X both make their appearance only after about 20% discharge when Reaction 5 begins to become important. The reaction becomes increasingly important as discharging continues until it becomes a dominating influence.

It can be concluded that the generally accepted electrochemistry for the alkaline Zn–MnO_2 cell adequately describes the behaviour of most states of charge. When discharged in excess of 80%, the cell impedance behaviour becomes inconsistent for each cell which makes interpretation difficult. It is considered that this is due to the deterioration in the well-ordered structure of the physical system.

Table 1.

Discharge (%)	*Open-circuit voltage* (V)	R_e (Ω)	θ_z (Ω)	C_z (F)	σ (Ω $s^{-1/2}$)	γ	θ_m (Ω)	C_m (F)	R_X (Ω)	C_X (F)
0	1.573	0.274	0.0071	0.21	0.047	0.74	–	–	–	–
5	1.501	0.299	0.0189	0.051	0.039	0.78	–	–	–	–
10	1.466	0.389	0.0201	0.078	0.039	0.80	–	–	–	–
20	1.418	0.295	0.0315	0.00195	0.039	0.85	0.0216	0.0409	0.014	2.467
30	1.374	0.310	0.0405	0.00130	0.064	0.7	0.0369	0.0310	0.024	0.6417
50	1.324	0.32	0.0928	691×10^{-6}	0.071	0.6	0.0498	0.0196	0.0623	0.350
60	1.287	0.349	0.1198	663×10^{-6}	0.0478	1.0	0.0197	0.0197	0.0987	0.307
70	1.246	0.360	0.1464	461×10^{-6}	0.0696	0.9	0.0598	0.0190	0.1109	0.335
80	1.188	0.4	0.1964	370×10^{-6}	0.156	0.3	0.203	0.0135	–	–

Acknowledgement

This work has been carried out with the support of Procurement Executive, Ministry of Defence.

References

[1] S. A. G. R. Karunathilaka, N. A. Hampson, R. Leek, T. J. Sinclair, *J. Appl. Electrochem.* **11** (1981) 365.
[2] *Idem, ibid* **10** (1980) 799.
[3] F. L. Tye, in 'Electrochemical Power Sources', (edited by M. Barak) Peter Peregrinus (for the IEE), London (1980) Ch. 3.
[4] J. E. B. Randles, *Disc. Faraday Soc.* **1** (1947) 11.
[5] H. Gerischer, *Z. Phys. Chem.* **158** (1951) 286.
[6] *Idem, ibid* **201** (1952) 55.
[7] H. A. Laitinen and J. E. B. Randles, *Trans. Faraday Soc.* **51** (1955) 54.
[8] S. A. G. R. Karunathilaka, N. A. Hampson, R. Leek and T. J. Sinclair, *J. Appl. Electrochem.* in press.